Indium-oxide polymorphs from first principles: Quasiparticle electronic states

F. Fuchs and F. Bechstedt

Institut für Festkörpertheorie und Optik and European Theoretical Spectroscopy Facility (ETSF), Friedrich-Schiller-Universität, Max-Wien-Platz 1, 07743 Jena, Germany

(Received 14 December 2007; revised manuscript received 11 February 2008; published 4 April 2008)

The electronic structure of In_2O_3 polymorphs is calculated from first principles using density functional theory (DFT) and many-body perturbation theory (MBPT). DFT calculations with a local exchange-correlation (XC) functional give the relaxed atomic coordinates of the two stable polymorphs. Their electronic structure, i.e., the band structure and density of states, is studied within MBPT. The quasiparticle equation is solved in two steps. As the zeroth approximation for the XC self-energy the nonlocal potential resulting from a HSE03 hybrid functional is used. In the sense of a self-consistent procedure G_0W_0 quasiparticle corrections are computed on top. The calculated direct quasiparticle gaps at Γ amount to 3.3 eV (rhombohedral) and 3.1 eV (cubic). The rhombohedral polymorph is found to exhibit a near degeneracy of the valence-band maxima at the Γ point and on the Γ-L line, while the valence-band maximum of the cubic polymorph occurs near Γ. Interconduction band transitions are identified as possible origin of conflicting experimental reports, claiming a much larger difference between the direct and indirect gap. The results for gaps, d-band positions, and density of states are compared with available experimental data.

DOI: 10.1103/PhysRevB.77.155107 PACS number(s): 61.50.Ah, 71.15.Nc, 71.20.−b, 71.15.Qe

I. INTRODUCTION

Indium oxide films are widely used for transparent electrodes in optoelectronics, e.g., solar cells, display devices, etc.[1] Recently, also nanostructures such as nanobelts[2] and nanotubes[3] have been realized on the basis of indium oxide. Especially tin-doped In_2O_3 exhibits a unique combination of optical and electrical transport properties such as high optical transparency in the visible range and low resistivity. Thereby, especially its conductivity strongly depends on the doping level, the manufacturing technique used, and the substrate temperature during growth and postdeposition treatments.[1,4] Given the observed high sensitivity of In_2O_3 properties on processing combinations, theoretical studies prove helpful in the clarification of the material properties of pure In_2O_3.

Despite their importance, however, even key quantities of the electronic band structure are not well known or under discussion. The majority of studies indicate an optical gap of about 3.5–3.8 eV.[1] Recent experimental studies combining different methods for thin In_2O_3 films[4] show a direct band gap of 3.5 ± 0.1 eV and an indirect band gap of 2.1 ± 0.2 eV. While the Γ point position of the direct gap is widely accepted, the magnitude of the indirect gap and the location of the valence-band maximum (VBM) in the Brillouin zone (BZ) are still under discussion.[5,6] One difficulty in the determination of the gaps is related to the existence of a depletion layer with a surface Fermi level between 2.2 and 3.5 eV above VBM.[5,7,8] In contrast, a small indirect gap would be consistent with a depletion layer-free flatband situation at the surface.

Besides several spectroscopic and optical measurements to elucidate the electronic structure of indium oxide, first-principles calculations can help us to investigate and understand its electronic properties. Indeed, recently such calculations have been performed.[9–13] However, several open questions and problems remain. Despite the fact that the results obtained are in overall agreement with available spectroscopic data, the reliability of the applied atomic sphere approximation (ASA)[9] or variational X_α method[10] is questionable because of the use of empirical parameters. Moreover, cluster calculations[10] are unlikely to describe the properties of crystals with a huge atomic basis in the elementary cell. The density functional theory (DFT) calculations with a local or semilocal approximation of the exchange-correlation (XC) energy functional[11–13] give rise to a typical underestimate of electronic excitation energies such as energy gaps.[14] This fact occurs independently of the used local density approximation (LDA) or generalized gradient approximation (GGA). The excitation aspect and hence the quasiparticle (QP) character of the electronic excitations are missing.

For In_2O_3, the gap underestimation is enhanced by the presence of shallow In 4d electrons and their underbinding in LDA or GGA. The hybridization of the In 4d and the O 2p states near the VBM gives rise to a pd repulsion and hence a gap shrinkage,[15] which is overestimated in LDA/GGA. For another In compound, InN crystallizing in wurtzite or zinc-blende structure, this hybridization effect between In 4d and anion p states was analyzed in detail.[16] An empirical scissors operator[14,17] can open the gaps but does not modify the band dispersion and thus cannot yield the correct band structure. In order to correct for the underbinding of the In 4d electrons within DFT-LDA or -GGA, the LDA+U and GGA+U methods have been applied to In_2O_3 recently.[12] There the self-interaction in the 4d shell is corrected for by taking into account an empirical Coulomb interaction parameter U. Nevertheless, the energy gaps remain too small since the excitation aspect is not included in the electronic-structure calculation. The parameter U is found to influence the position of the VBM in $\mathbf{k}$ space and hence the relation between the direct and indirect band gaps.

A remaining open question is the influence of the actual crystallographic structure of In_2O_3 on the electronic bands. The majority of electronic structure calculations have only been performed for one polymorph, mostly for a cubic bixbyite-type structure.[9–12,15] There is only one paper[13] that

studies the influence of the bonding behavior and coordination on the electronic structure, as well as the optical and transport properties, for rhombohedral and cubic In_2O_3. It, however, remains within the framework of DFT-LDA and GGA.

In the present paper, we study the stability of three crystalline In_2O_3 phases. For the two stable polymorphs, the electronic band structure is calculated in different approximations: the DFT-LDA, an approach using a hybrid XC functional for which the resulting spatially nonlocal potential can be interpreted as a first approximation to the XC self-energy, and a quasiparticle description on top of the eigenvalues and eigenfunctions of the hybrid functional calculation. A brief description of the used methods is given in Sec. II. In Secs. III and IV, we discuss the results for the atomic and band structures. In Sec. V, the consequences and reliability of the different approximations are discussed for the density of states, gaps, 4*d*-band positions, and optical properties. The results are compared with available experimental data. Finally, Sec. VI contains the summary and conclusions.

II. COMPUTATIONAL METHODS

All the calculations are performed using the Vienna *ab initio* simulation package (VASP).[18–20] The projector-augmented wave method[21,22] is used to model the electron-ion interaction. Usually it allows for the accurate treatment of first-row elements such as oxygen and localized states such as In 4*d* at modest plane-wave cutoffs. For In_2O_3, however, we found the convergence with the number of plane waves to be rather slow. Therefore, plane waves up to a kinetic energy of 550 eV are included in the expansion of the electronic wave functions, throughout this work. The BZ integrations are performed by summations over special points of the Monkhorst–Pack type.[23]

In the present study, a large variety of material properties are addressed. In principle, we distinguish between ground-state and excited-state calculations. The ground-state calculations, addressing the energetic stability of In_2O_3 polymorphs and their equilibrium structures, are performed throughout in the framework of DFT,[24,25] using the spatially local LDA-XC functional of Perdew and Zunger.[26] Monkhorst–Pack meshes of $5\times5\times5$ **k** points for the cubic, $8\times8\times8$ for the rhombohedral, and $8\times8\times3$ for the hexagonal unit cell are found sufficient to converge the atomic coordinates. The relaxed atomic geometries and lattice parameters are obtained my minimizing the total energy. For the final structures, the forces acting on the ions are well below 1 meV/Å.

The excited-state properties, in principle, should be studied consistently in the framework of many-body perturbation theory (MBPT). However, the computational effort for this is prohibitive at the moment due to the large unit cells found for In_2O_3. Therefore, three different methods are used to study the electronic structure. As a first approach, we use the Kohn–Sham[25] eigenvalues in Sec. IV A. Beside the well-known gap underestimation, they can give a first impression of the band structure and the electronic density of states (DOS), and yield insight in the relationship between atomic geometry and bonding to the electronic states. The corresponding BZ integrations are performed using the tetrahedron method[27] with **k**-point meshes of $14\times14\times14$ for the cubic and $20\times20\times20$ **k** points for the rhombohedral structure. The same **k**-point meshes are used for the calculation of optical properties in the independent-(quasi)particle approximation[28] in Sec. V. Furthermore, to account for finite lifetimes, the resulting spectra are broadened by 0.2 eV, and a scissors operator of 1.99 eV is used to widen the gap toward the HSE03+G_0W_0 calculated in Sec. IV B. Excitonic effects are not included in the calculations.

In order to obtain the true single-particle excitation energies, one has to solve the so-called QP equation.[14] Formally, it is similar to the Kohn–Sham (KS) equation.[25] However, the local XC potential V_{XC} is replaced by a nonlocal, non-Hermitian, and energy-dependent XC self-energy Σ. This self-energy is approximated by *GW*, i.e., by its first-order expansion in the dynamically screened Coulomb potential *W*, as suggested by Hedin.[29] The factor *G* denotes the single-particle Green's function. Since the DFT-LDA gaps for In_2O_3 (Refs. 9 and 11–13) are only fractions of the experimental ones, the usual perturbation-theory treatment (called G_0W_0) of the operator $(\Sigma-V_{XC})$ is of very limited success when the KS electronic structure is used as a starting point. A self-consistent solution of the QP equation can overcome this problem: however, it is prohibitively expensive for systems as large as In_2O_3. Therefore, we use a computationally more efficient approach with a nonlocal hybrid XC functional as a starting point for the solution of the QP equation. This was recently shown to give reliable estimates for fundamental gaps and *d*-band binding energies.[30] Explicitly, we use the HSE03 hybrid XC functional[31] which contains a screened exchange interaction and thereby models part of the QP self-energy Σ.

In Sec IV B, we study the quasiparticle effects for the band structure and the DOS of different In_2O_3 polymorphs, comparing the approximations DFT-LDA, HSE03, and HSE03+G_0W_0 (only for the rhombohedral polymorph). For the latter two, the DOS is calculated upon eigenvalues computed on an $8\times8\times8$ **k**-point mesh. Thereby, a reduced sampling of $4\times4\times4$ **k** points is used for the calculation of the exchange kernel and the dielectric matrix (in W_0). The band structures are calculated along high-symmetry directions using the same exchange kernel. In the case of HSE03+G_0W_0, the energy bands are computed only at a comparably small number of **k** points, due to the numerical costs. To converge the dielectric screening 468 conduction bands are used in the G_0W_0 calculation. Furthermore, the band structures are compared to the results of LDA+U^3 (Ref. 32) calculations, computed in the approximation of Dudarev *et al.*[33] A value of 5 eV was chosen for the *U* parameter in order to shift the In 4*d* states to −14.3 eV, close to the measured position[7,8] and the HSE03+G_0W_0 result.

III. GROUND-STATE PROPERTIES

A. Atomic geometry

According to the inorganic crystal structure database (ICSD),[34] In_2O_3 is reported to exist in three different crystal

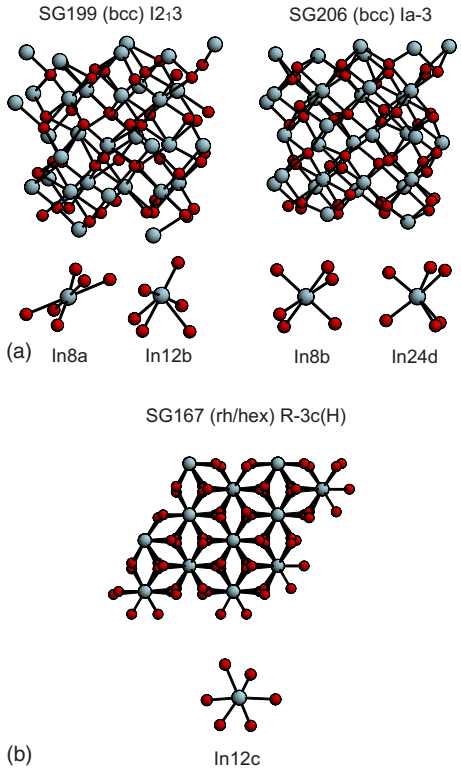

FIG. 1. (Color online) Bonding geometries (upper panels) of the three In_2O_3 polymorphs studied. In atoms: large blue/light gray circles; O atoms: small red/gray circles. The local arrangement of In and O atoms in the building blocks is shown in the lower panel.

structures: two body-centered cubic (bcc) structures *SG*199 and *SG*206 as well as a rhombohedral (rh) one *SG*167. Besides the different Bravais lattices, bcc or rh, these polymorphs possess different space groups: $I2_13$(*SG*199), $Ia\bar{3}$(*SG*206), and $R\bar{3}c$(*SG*167). Their bonding geometries are indicated in Fig. 1. The oxygen atoms are twofold coordinated in all In_2O_3 geometries. The coordination of the In atoms is also given. In the *SG*199 case, the two types of In atoms are surrounded by oxygen in octahedral and trigonal prismatic coordinations, respectively. The bonding polyhedra slightly differ in the *SG*206 structure. The cubic polymorphs feature a primitive unit cell with 8 In_2O_3 units, i.e., 40 atoms, and both represent bixbyite-type crystal structures. The corresponding simple cubic cells have an edge length of a_0. The structure with the space group $Ia\bar{3}$ is sometimes also described as a *C*-type rare-earth structure, which is similar to a fluorite geometry but every fourth anion is missing.[1] Another polymorph, the corundum structure, is formed when the In atoms are surrounded by oxygen in a trigonal biprism coordination. This polymorph has *SG*167 symmetry with two In_2O_3 formula units, i.e., 10 atoms, in the primitive rhombohedral unit cell with the lattice constants a and c. This polymorph may also be described by nonprimitive unit cells of a hexagonal Bravais lattice. The nonprimitive unit cells contain six In_2O_3 units, i.e., 30 atoms. Test calculations using the non-primitive hexagonal unit cell revealed that the relaxed atomic positions are identical to those relaxed in the rhombohedral setting.

In order to determine the equilibrium lattice parameters, the total energies are calculated for varying volumes, allowing for the relaxation of all internal parameters and the unit cell shape. Doing so, the cubic *SG*199 polymorph is found to be unstable. The relaxation of the corresponding starting geometry automatically yields the bonding arrangement of the *SG*206 polymorph. There is no energy barrier for this process. This finding is in agreement with the result of similar calculations.[13] Consequently, we restrict our studies to the bcc *SG*206($Ia\bar{3}$) and rh *SG*167($R\bar{3}c$) polymorphs in the following.

The resulting lattice parameters and atomic positions in Wyckoff notation are listed in Table I. The computed lattice constants are in excellent agreement with experimental values $a_0=10.117$ Å and $a=5.487$ Å, $b=14.510$ Å.[34] The small discrepancies are related to the overbinding effect in the DFT-LDA. In the case of the bcc polymorph, such an agreement also holds for the comparison with other first-principles calculations: $a_0=10.00$,[11] 10.33,[35] and 10.077 Å.[12,13] For the rhombohedral structure with $a=5.59$ Å, $c=14.87$ Å (Ref. 35) or $a=5.493$ Å, $c=14.424$ Å,[13] the agreement is also satisfying taking into account the trend of lattice-constant overestimation observed within DFT-GGA.[35] Also, the atomic coordinates given in Ref. 13 agree well with those in Table I.

B. Energetics

The structural parameters are derived from the energy-volume dependencies in Fig. 2 calculated for the two stable polymorphs. They are fitted against the Murnaghan[36] and for comparison the Vinet[37] equation of state (EOS) to extract the equilibrium volume, cohesive energy, bulk modulus, and its

TABLE I. Structural and energetical parameters of stable In_2O_3 polymorphs.

Polymorph	Lattice parameter (Å)	Atomic coordinates in Wyckoff notation				B (GPa)	B'	Cohesive energy per formula unit (eV)
		Atom type	x	y	z			
bcc	$a_0=10.094$	In 8*b*	0.2500	0.2500	0.2500	174	4.60	28.33
*SG*206		In 24*d*	0.4665	0.0000	0.2500			
		O 48*e*	0.3901	0.1543	0.3818			
rh	$a=5.479$	In 12*c*	0.0000	0.0000	0.3577	176	4.24	28.22
*SG*167	$c=14.415$	O 48*e*	0.2954	0.0000	0.2500			

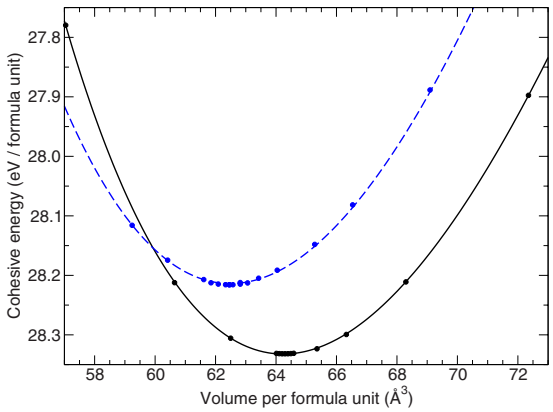

FIG. 2. (Color online) Cohesive energy versus volume (both per formula unit, f.u.=In_2O_3). Solid line: bcc phase; dashed line: rh phase. Circles indicate volumes actually sampled by the calculations.

pressure derivative. Since the values of the above mentioned fitting parameters were found to agree for converged plane-wave cutoffs and **k**-point meshes, only one value is given in Table I.

From Table I and Fig. 2, it can be seen that the bcc polymorph has the lowest total energy and is thus predicted to be stable under ambient conditions in accord with experimental observations. The rhombohedral In_2O_3 is usually identified as a high-pressure phase,[38] although it can also be grown using metal organic chemical vapor deposition.[39] The bonding in In_2O_3 is strong with a cohesive energy of about 5.67 eV/at. Comparable values are found for other oxides with dominantly ionic bonding such as MgO (5.01 eV/at.).[40] Similar studies[12,13] report even larger cohesive energies. This may be related to a different choice of the atomic reference energies. We take into account spin polarization in the calculation of the atomic reference energies of the free atoms. Without correction, the total energy per f.u. calculated for the bcc polymorph amounts to −31.8 eV. The isothermal bulk moduli B in Table I are also in agreement with other recent calculations.[12,13] The rather, small values of the pressure derivatives B' of about 4.2–4.6 indicate well-converged computations. Test calculations of the total energies with a plane-wave cutoff smaller than 550 eV gave rise to jagged energy over volume curves and, consequently, to less defined parameters B and B' in the EOS fit.

IV. EXCITED-STATE PROPERTIES

A. Bands and bonds

The Kohn–Sham eigenvalues are directly related to the atomic geometries described above. Despite of the missing excitation aspect, the corresponding DFT-LDA energy-band structures and the corresponding density of states, especially the partial DOS resolved with respect to a certain orbital symmetry, yield important information about the band dispersion and the bonding character. The corresponding bands and accompanying density of states for the bcc and rh

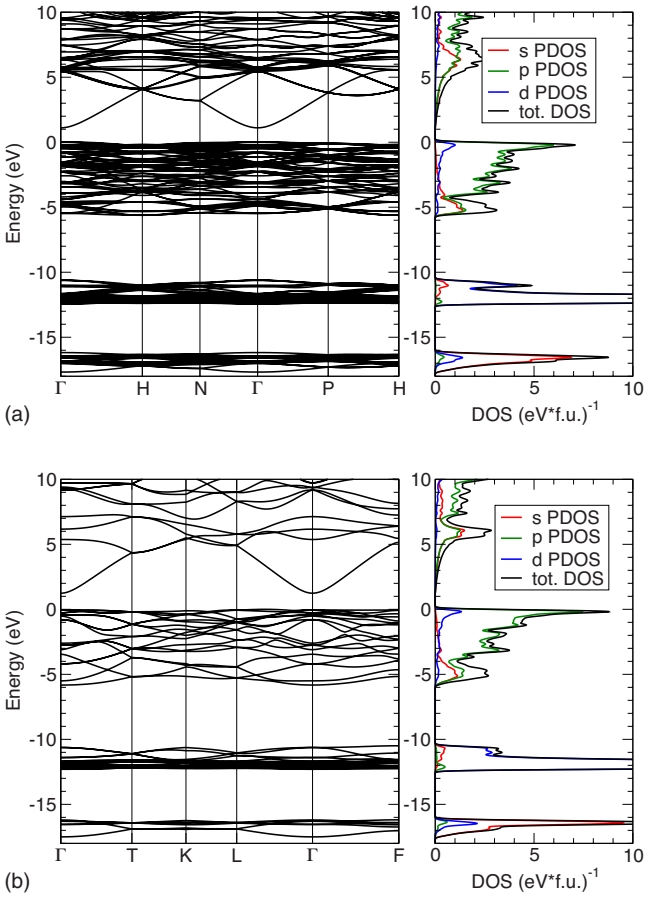

FIG. 3. (Color online) Band structures, DOS, and s,p,d projected partial DOS of the bcc (a) and rh (b) polymorphs of In_2O_3 calculated within DFT-LDA. The DOS is normalized to the number of states per energy interval and f.u. The VBM is used as energy zero.

polymorphs are shown in the upper and lower panels of Fig. 3, respectively. Independent of the polymorph, the most striking features of the band structures are the pronounced **k** dispersion of the lowest conduction band near Γ (similar to other In compounds),[16] the mainly O 2p-derived uppermost valence bands with a bandwidth of about 6 eV, the In 4d-related bands in the energy range −11 to −13 eV, and the lowest O 2s-derived narrow valence bands. The band-structure details are more complex due to the hybridization of different atomic orbitals. For instance, the lowest conduction band starts with a pure In 5s character but mixes in In 5p character with increasing **k** vector. The uppermost parts of the valence bands are influenced by hybridization with In 4d states. Due to the LDA-typical underestimation of the In 4d binding energies, the coupling and admixture of O 2p and In 4d states are overestimated in the present calculations leading to about 20% d character for the VBM.

For both polymorphs, the conduction band minimum is found at the Γ point.The VBM, however, lies close to the Γ point on the Γ-H line for the bcc polymorph, while it is found significantly off Γ, approximately midway between Γ and L, for the rh polymorph. The fundamental (indirect) gaps amount to 1.12 eV (bcc) and 1.27 (rh). The direct gaps at the

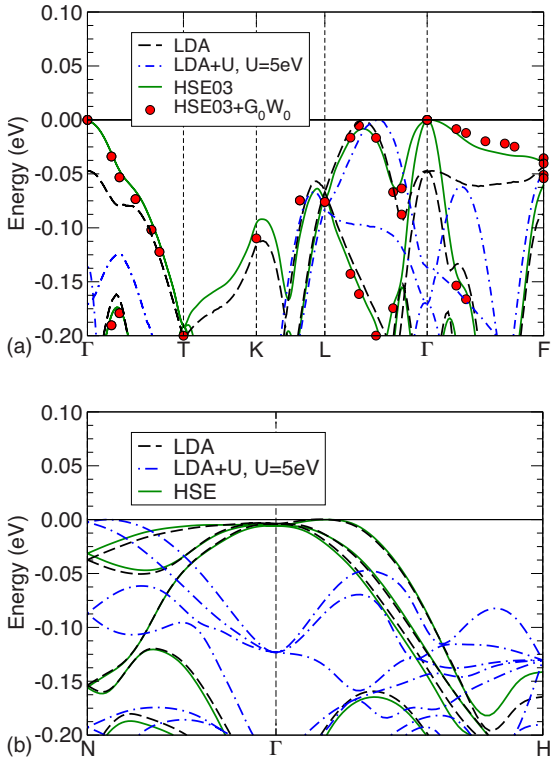

FIG. 4. (Color online) Valence-band structures of rh (a) and bcc (b) polymorphs, calculated within the DFT-LDA (dashed, black), LDA+U (dash-dotted, blue/dark gray), and HSE03 (solid, red/gray) approximations for XC. For the rh polymorph, also the HSE03 $+G_0W_0$ quasiparticle band structure is given (black dots). The VBM is used as energy zero.

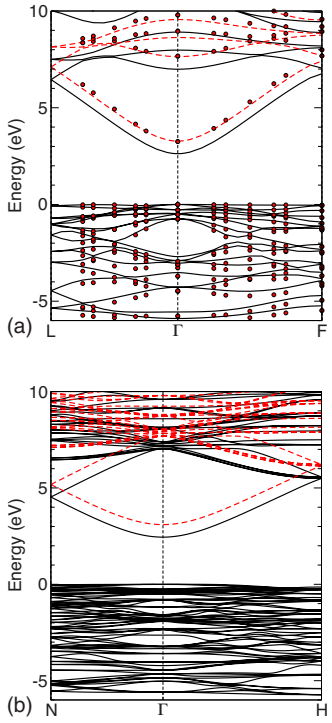

FIG. 5. (Color online) Quasiparticle band structures of the rh (a) and bcc (b) In_2O_3 polymorphs. Solid lines (black): HSE03, dots (red/gray): HSE03+G_0W_0, and dashed lines (red/gray): HSE03+Δ conduction bands. The VBM is used as energy zero.

Γ point are only slightly larger by less than 10 meV (bcc) or about 40 meV (rh). Indeed, the whole upper valence band shows only a small dispersion with a total variation of about 200 meV, leading to a sharp peak in the DOS at the valence-band edge. This peak is slightly more pronounced in the case of the rh polymorph. Apart from that, however, the DOS of the two polymorphs differs very little concerning the general line shape and peak positions. Only a small shift of 0.1 eV toward higher binding energies is found for the In 4d-band related DOS peak of the bcc polymorph with respect to the rh one, and small differences occur for the DOS derived from the conduction bands (cf. Fig. 3). Due to the similar approaches, the DOS calculated in this work for the bcc polymorph is largely identical to that published by Erhart *et al.*[12] There, also the use of an additional semiempirical potential U acting on the d states was studied. This can be used to reduce pd coupling by increasing the d-band binding energies. For the bcc polymorph, such a procedure results in a slightly different dispersion for the topmost valence band, moving the VBM somewhere near the N point on the Γ-N line (see also Fig. 4). The difference of the direct gap at the Γ point and the fundamental gap is increased but remains below 50 meV.[12] A definite prediction for the **k** space and energy position of the band extrema, however, can only be given taking into account the excitation aspect.

B. Quasiparticle electronic structure

The QP calculations include two steps. Instead of the DFT-LDA electronic states, in the first step we evaluate the band structures using the HSE03 hybrid XC functional,[31] expecting band energies to be close to the QP ones. In the second step, we compute the G_0W_0 XC self-energy by means of the HSE03 eigenfunctions and eigenvalues. Obtaining convergence is already a challenge for the rh polymorph with 10 atoms and 88 electrons in a unit cell. Currently, for the bcc polymorph, this procedure is almost prohibitively expensive due to the large unit cells with 40 atoms and 352 electrons. For that reason, in the bcc case, we present the HSE03 results. The QP effects are taken into account by a scissors operator Δ that shifts the conduction bands toward higher energies. The value for $\Delta=0.65$ eV is obtained from the gap opening computed for the rh polymorph. Given the agreement between the HSE03+Δ and HSE03+G_0W_0 bands, demonstrated in Figs. 5(a) and 4(a), the HSE03+Δ approximation should represent a good approximation for the QP band structure in the energy region around and close to the gap. Even for the rh structure, the QP band structure can only be calculated at a comparably small number of **k** points, due to the numerical costs. However, it still allows for a reasonable presentation of the DOS as well as the band structure along a few high-symmetry directions. For both polymorphs, rh and bcc, the results are shown for the band structures in Fig. 5 and the DOS in Fig. 6. Apparently, the QP effects are almost negligible for the uppermost valence bands, at least in case of the HSE03 starting point and the use of the VBM as

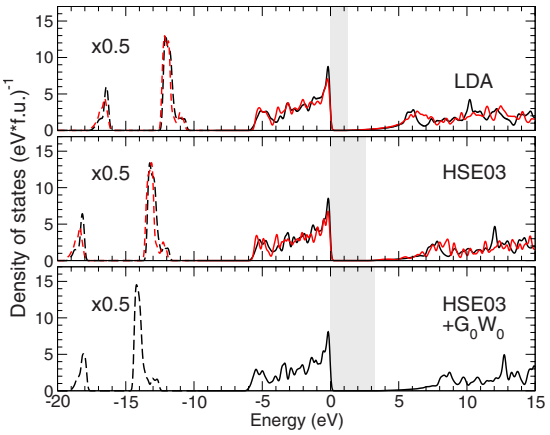

FIG. 6. (Color online) Density of states of the rh (black) and bcc (red/gray) In_2O_3 polymorphs in three (two for the bcc polymorph) different approximations for exchange and correlation: LDA, HSE03, and HSE03+G_0W_0. In the energy region below 8 eV, the DOS was rescaled by a factor 0.5 to allow for a common scale with the DOS around the VBM. The rescaled DOS is shown as a dashed line. The gray shaded region indicates the fundamental gap. The VBM is used as energy zero.

the common energy zero. In this energy range, the most important QP effect is the shift of the conduction bands toward higher energies, which is almost constant for all **k** points. The width 5.8 eV of the uppermost valence bands remains almost unaffected by the many-body effects.

The fundamental gaps resulting from the HSE03+G_0W_0 (Δ for bcc) scheme are 3.26 and 3.10 eV for the rh and the bcc polymorphs, respectively. These values are seemingly somewhat smaller than the experimental values reported.[1] However, it is not certain whether these differences are due to a lack in the theoretical or experimental treatment. On the one hand, the *pd* repulsion may still be slightly overestimated (see discussion above), causing an underestimated gap. On the other hand, the experimental determination of the gap might suffer from the extremely low density of states near the conduction-band minimum. This makes the determination of the gap by optical-absorption measurements difficult. Recently, Wang *et al.*[39] discussed that the direct gaps derived from optical-absorption spectra approach values of 3.0 eV for the rh polymorph and 3.7 eV for the bcc structure. These values envelope the computed gaps; however, they are influenced by the extremely low joint density of states at the gap (see the discussion in Sec. V).

Figure 6 demonstrates the influence of the many-body effects for a wider energy range. Explicitly, the density of states is plotted for both stable polymorphs in three different approximations for the XC self-energy. While the modifications in the density of the uppermost valence states are small, the HSE03 DOS shows a remarkable redistribution in the higher-energy region of the conduction bands. In addition, significant shifts to lower energies (or larger binding energies) occur for the mainly In 4*d*- and O 2*s*-derived bands. These shifts amount to 1.1 eV (In 4*d*) and 1.7 eV (O 2*s*). The quasiparticle effects in the density of valence states mainly affect the In 4*d* peak. It is shifted toward lower energies (i.e., larger binding energies) by 1.0 eV, in the rh case. The calculated In 4*d* binding energy amounts to 14.2 eV with respect to the VBM. This value is in good agreement but at the lower limit of the reported range of binding energies: 14.0–15.5 eV measured by synchrotron-radiation-excited photoelectron spectroscopy.[7,8] Consequently, there might remain a small gap underestimation, due to the slight overestimation of the *pd* repulsion.[30] The overall DOS line shape is similar to experimental spectra, combining results of x-ray photoemission and Bremsstrahlung isochromat spectroscopy (see Fig. 3 of Ref. 9).

C. Electron effective masses and Burstein–Moss shift

From the band-structure data in Fig. 5, it is possible to extract the effective masses of the first conduction band, at least in the LDA and HSE03 approximations for XC. For the quasiparticle band structure, too few **k** points are available for a reliable fit. However, close to the conduction-band minimum (CBM), the dispersion is found to be changed little by the QP corrections. Consequently, the HSE03 results may be interpreted as the correct values for the quasielectrons near Γ. For the bcc polymorph, the effective electron mass at Γ is almost isotropic and amounts to $m^*=0.18/0.22m_0$ (LDA/HSE03). For the rh polymorph, $m_x^*=m_y^*=0.16/0.22m_0$ and $m_z^*=0.16/0.23m_0$ (LDA/HSE03) are the two independent elements in the tensor of effective masses. The difference between both is found to be very small indicating an almost vanishing anisotropy.

The almost vanishing anisotropy and the mass value of $0.16m_0$ in the rh case agree very well with other recent DFT-GGA results.[13] In the bixbyite case, the GGA approach gives slightly larger masses of about $m^*=0.20\cdots0.23m_0$ than the LDA used here. Within the pseudopotential approximation, even higher effective masses of $0.34m_0$ are reported.[17] Our quasiparticle (HSE03) values at Γ approach the experimental values of $m^*=0.28\cdots0.35m_0$[1,41] derived from optical measurements of the Drude term to free carriers. These results, however, are influenced by the value of the static dielectric constant and the parabolic approximation of the conduction band used in calculation of m^*. Especially the approximation of a **k**-independent mass m^* seems questionable in the light of our data. Although the conduction-band nonparabolicity of In_2O_3 is smaller than in other In compounds, e.g., InN, the **k** dependence of the effective mass is not negligible. In case of the cubic polymorph, a more accurate approximation for the conduction band,

$$E_c(\mathbf{k}) = \frac{1}{2}\left[E_g + \sqrt{E_g^2 + 4\left(\frac{m_0}{m^*} - 1\right)E_{\mathbf{k}}E_g}\right] + E_{\mathbf{k}}, \qquad (1)$$

with $E_{\mathbf{k}}=(\hbar^2/2m_0)\mathbf{k}^2$ and the (direct) gap energy E_g can be obtained from $\mathbf{k}\cdot\mathbf{p}$ theory.[16] Fitting the computed band structure against Eq. (1) does not change the values for the effective masses at Γ but reduces the deviations at larger **k**. From Eq. (1), it is clear that the **k**-dependent effective mass $m^*(\mathbf{k})$,

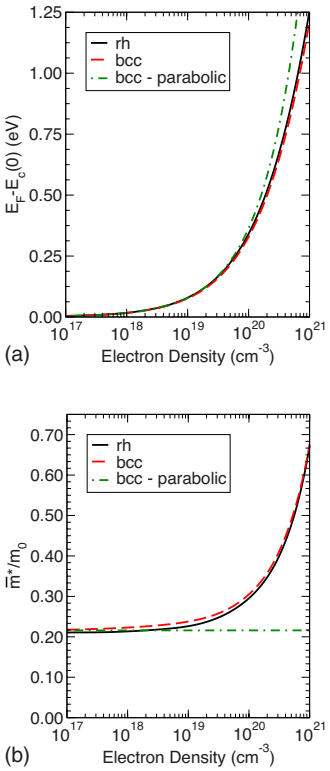

FIG. 7. (Color online) Burstein–Moss shift or Fermi level position (a) and average effective mass (b) as a function of the free-electron density calculated for the rh polymorph (solid, black) and the bcc polymorph (dashed, red/gray) from the HSE03 band structure. The parabolic approximation to the bcc conduction band is shown for comparison (dash-dotted, green/light gray).

$$\frac{m^*(\mathbf{k})}{m_0} = \left\{ 1 + \frac{m_0/m^*(0) - 1}{[1 + 4(m_0/m^*(0) - 1)E_\mathbf{k}/E_g]} \right\}^{-1}, \quad (2)$$

increases away from Γ. The nonparabolicity (1) of the conduction band also influences the Burstein–Moss shift, i.e., the position $E_F - E_c(0)$ of the Fermi level with respect to the CBM. This quantity is directly related to the free-electron density,

$$n(E_F) = \frac{2}{\Omega} \sum_\mathbf{k} \Theta(E_F - E_c(\mathbf{k})). \quad (3)$$

Figure 7(a) shows the strong nonlinearity of the Burstein–Moss shift with increasing free-electron density. However, the influence of the polymorph as well as of the nonparabolicity is rather small. This is completely different for the average and, therefore, density-dependent effective electron mass $\bar{m}^*$,

$$\frac{\bar{m}^*}{m_0} = \left[\frac{1}{n(E_F)} \frac{2}{\Omega} \sum_\mathbf{k} \frac{m_0}{m^*(\mathbf{k})} \Theta(E_F - E_c(\mathbf{k})) \right]^{-1}. \quad (4)$$

While the polymorph dependence remains small, the mass increases rapidly with the electron density [cf. Fig. 7(b)]. At a density of about $n = 10^{20}$ cm^{-3}, the average effective mass exceeds $\bar{m}^* > 0.3 m_0$ and, thereby, approaches the experimental values.

TABLE II. Direct gaps at the Γ point. The lowest indirect gaps are given in parentheses if available. All values are given in eV.

Polymorph	LDA	HSE03	HSE03+G_0W_0/Δ
SG167, rh	1.27 (1.23)	2.61 (2.57)	3.26
SG206, bcc	1.12 (1.11)	2.45 (2.44)	3.10

D. k-space position of valence-band maximum: Influence of many-body effects

In order to discuss the directness or indirectness of In_2O_3 in detail, we have studied the band structure for both stable polymorphs for energies close to that of the VBM. Three different approximations of the XC self-energy—LDA, HSE03, and HSE03+G_0W_0—are used. The corresponding gap results are given in Table II. In addition, we apply the LDA+U method analog to the study of Erhart *et al.*,[12] however, with a slightly smaller interaction parameter $U = 5$ eV. Furthermore, different from Ref. 12, we use the LDA-relaxed atomic positions in all the present calculations.

Figure 4 shows the corresponding band structures along the BZ path N-Γ-H for the bcc polymorph, and Γ-T-L-Γ-F for the rh polymorph. Interestingly, in the case of the bcc polymorph, the highest valence bands change extremely little switching from LDA to the HSE03. This contrasts the results of the present and other[12] LDA+U calculations that are found to lower the VBM at the Γ point and enhance the indirect gap–direct gap difference, compared to the LDA value for both polymorphs. For the rh structure, the use of LDA+U displaces the actual VBM position only slightly. Upon the use of the HSE03 XC functional, however, a new VBM arises at the Γ point. The resulting maxima of the upper valence band are basically degenerate, differing only by about 10 meV. Finally, Fig. 4(a) also includes the QP band structure for the rh polymorph resulting from an HSE03+G_0W_0 calculation. Comparing it to the HSE03 band structure again confirms that the difference between both is small for the upper valence bands.

E. Below-gap optical transitions due to *n* doping

From the band structures analyzed in the preceding sections, the differences between the direct and indirect gaps are found to be very small. Therefore, from the theoretical point of view, the energy difference of the two gaps of 1.4 eV,[4] as derived from a combination of scanning tunneling and optical measurements, has to be refused. One possible explanation for the optical absorption onset around 2.5 eV measured by Matino *et al.*[4] can be given taking into account the presence of free electrons, partially filling the lowest conduction band. This is schematically shown in (Fig. 8(a)). Beside the well-known effect of shifting the main onset of optical absorption ($E_{v\text{-}c}$) by the Burstein–Moss effect (cf. Sec. IV C), the particular band structure of In_2O_3 allows for the occur-

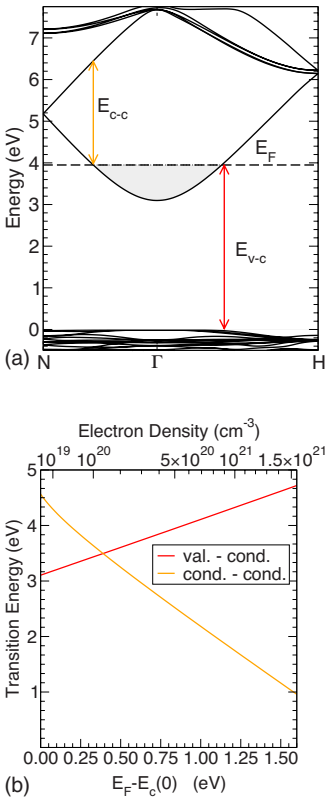

FIG. 8. (Color online) **k**-space location (a) and energy (b) of the lowest possible optical transitions depending on the Burstein–Moss shift or free-electron density calculated from the HSE03+Δ band structure of bcc-In_2O_3. The red/gray arrow in (a) and the red/gray line in (b) indicate the minimum transition energies between the upper valence band and the lowest conduction band. The orange/light gray arrow in (a) and the orange/light gray line in (b) indicate transitions between the two lowest conduction bands. The Fermi level is indicated schematically by a dashed line in (a).

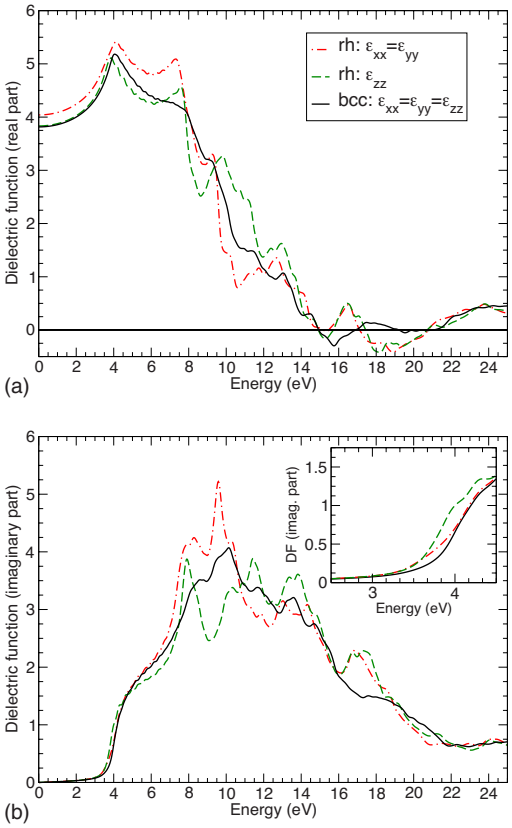

FIG. 9. (Color online) Real (a) and imaginary parts (b) of the dielectric function of In_2O_3. The scalar dielectric functions are shown for the bcc polymorph (solid, black) and the rh polymorph [ordinary (dash-dotted, red/gray) and extraordinary polarization (dashed, green/light gray)]. The inset in the lower panel shows the details of the absorption onset region.

rence of additional optical interband transitions between the lowest conduction bands at relatively low free-electron densities. According to Fig. 8(b), a new carrier-induced absorption edge $E_{c\text{-}c}$ related to interconduction band transitions may appear at lower energies for sufficiently high n doping with $n > 10^{20}$ cm^{-3}. Furthermore, an optical onset at 2.5 eV as seen in experiment[4] is expected at a carrier density of approximately 5×10^{20} cm^{-3}, agreeing very well with the free-electron density of 2.7×10^{20} cm^{-3} estimated there.

V. CONSEQUENCES FOR OPTICAL PROPERTIES

Figure 9 shows the real and imaginary parts of the dielectric function (DF) $\varepsilon(\omega)$ for both the bcc and rh polymorphs of In_2O_3 in the limit of vanishing free-electron densities. The dielectric functions are calculated in the independent-quasiparticle approximation (IQPA)[42] using the scissors-operator approach to compensate the gap underestimation found in the LDA. The scissors shift for the conduction bands is derived from the HSE03+G_0W_0 gap calculated for the rh polymorph in Sec. IV B. It amounts to 1.99 eV. We are mainly interested in the influence of the In_2O_3 crystal structure on the optical properties for photon energies $\hbar\omega < 20$ eV. According to the band structures in Fig. 3, this energy range is dominated by transitions from the dominantly p-symmetric valence bands, into the lowest conduction bands. From the experience with another In compound, InN, where the anions are also a first-row element,[16] we can expect that the quasiparticle effects in the lower-energy region are well represented by the scissors shift. The positions of the higher-energy peaks above 7 eV should be underestimated, compared to an IQPA spectrum using GW-derived QP shifts instead of the scissors approximation. However, excitonic effects, which are not included in our computations, give rise to a redshift accompanied by a certain redistribution of spectral strength from higher to lower photon energies.[16] Therefore, the higher-energy peak positions might agree quite well with the experimental values due to some error compensation between the scissors approximation and the neglect of excitonic effects.

The spectral variation is best characterized by the frequency dependence of the imaginary part of the DFT in Fig. 9. It is similar to that described by Karazhanov *et al.*[13] The spectra can be divided in three energy regions: the absorption onset between 3 and 4 eV, a transition region between 4 and 7 eV with increasing spectral strength, and a region of absorption peaks above 7 eV, which exhibits a sig-

nificant polarization anisotropy for the rh polymorph but also a strong dependence on the polymorph, rh or bcc. The inset in Fig. 9 shows that the steep absorption onset starts well above the quasiparticle gap. The high-energy peaks may be related to contributions from high-symmetry points and lines in the BZ to the joint density of states. Apparently, the dielectric functions resemble each other closely in the low-energy part of the spectrum up to 7.0 eV. At higher energies, the DF of the rh polymorph shows a modified peak structure with additional or more pronounced peaks at 8.0, 9.6, 11.5, 13.7, and 17.0 eV.

It is interesting to compare the onsets of the imaginary DF of both polymorphs, noticing a redshift of about 0.2 eV for the rh DF against the bcc one. This is due to the influence of the optical transition matrix elements, which remain comparably small up to 1 eV above the gap energy for the bcc structure while they increase right away from the gap for the rh structure. One should note that this ordering of the absorption edges opposites the ordering of the fundamental gaps (cf. Table II). Thus, by means of absorption measurements, a smaller edge position should be derived for the high-pressure rh phase than for the bcc polymorph. Indeed, this has been observed experimentally.[39] On the other hand, for both the bbc [41] and the rh[39] polymorphs, the measured optical absorption seems to be much higher than the theoretical predictions. This enhancement may be related to the presence of free carriers in the lowest conduction band of the investigated samples.

The real parts of the DF in Fig. 9(a) reflect several features from the imaginary parts because of the Kramers–Kronig relation. The vanishing frequency value in the DF defines the static electronic dielectric constant by $\varepsilon_\infty = \mathrm{Re}\,\varepsilon(\omega=0)$. According to the results in Fig. 9(a), the static electronic dielectric constants amount to 3.82 for the bcc polymorph, 4.04 for the ordinary, and 3.83 for the extraordinary DF of the rh polymorph, respectively. These values approach the experimental dielectric constant of about $\varepsilon_\infty \approx 4.0$.[1] Another interesting feature in the real parts are their zeros, $\mathrm{Re}\,\varepsilon(\omega)=0$, near $\hbar\omega=15$, 17, and 21 eV. They represent the energies of plasmonic excitations. The lower energies approach the free-electron plasma frequency of the electrons occupying the O $2p$ bands. The high-energy zeros may be influenced by the contributions from In $4d$ states.

VI. SUMMARY AND CONCLUSIONS

The electronic structure of In_2O_3 polymorphs and its consequence for other properties have been studied from first principles. The density functional theory in its local version has been applied to optimize the atomic equilibrium geometries and to study the stability of the three polymorphs with space groups $I2_13$, $Ia\bar{3}$, and $R\bar{3}c$. The electronic structure was studied on basis of the hybrid HSE03 XC functional, giving rise to band structures that agree quite well with QP band structures—except for a small gap underestimation. Quasiparticle energies have been computed for the rh polymorph in a perturbative approach within the framework of Hedin's GW approximation. Since this is computationally too expensive for the cubic polymorph with 40 atoms in the primitive unit cell, we employed the scissors-operator approach there, however, using a parameter-free determined value for the scissors shift. For the purpose of comparison, strong correlation effects in the In d shell have been studied as well within the LDA+U approximation.

During the ionic relaxation, the cubic polymorph with $I2_13$ symmetry has been found to be unstable. The other bcc polymorph and the high-pressure rh phase are found to give rise to rather similar electronic structures, especially densities of states. The QP calculations show that the polymorphs are slightly indirect (bcc) or the direct and direct gaps are almost degenerate (rh). In any case, In_2O_3 does not possess an indirect gap significantly smaller than the direct one as indicated by some experiments. The calculated direct quasiparticle gaps amount to 3.1 eV (bcc) and 3.3 eV (rh). This corresponds to quasiparticle gap corrections of about 0.65 eV (1.99 eV) with respect to the HSE03 hybrid functional (Kohn–Sham) values. Also, the ln $4d$ and O $2p$ bands are significantly shifted toward larger binding energies by about 0.9/0.9 eV (2.1/2.5 eV) compared to the HSE03 hybrid functional (Kohn–Sham) values. Their quasiparticle excitation energies with respect to the VBM are with 14.3 and 18.5 eV close to binding energies measured by photoelectron spectroscopy. The influence of n doping is discussed in detail, studying the Burstein–Moss effect and the occurrence of additional interconduction band transitions.

Furthermore, we have calculated the frequency dependence of the dielectric functions in the independent-quasiparticle approximation. It leads to static electronic dielectric constants of about $\varepsilon_\infty=4.0$ in agreement with experimental data. The spectral behavior of the imaginary part of the dielectric functions is characterized by a steep absorption onset followed by a weakly varying part. Above photon energies of 7.5 eV, several peaks are visible due to Van Hove singularities in the joint density of states. The spectra depend on the polymorph and the light polarization (in the rhombohedral case). The strongest variations occur near the absorption onset and the peak regions below and above photon energies of 10 eV. They may be useful to distinguish between polymorphs.

ACKNOWLEDGMENTS

Discussions with J. Furthmüller and G. Kresse are gratefully acknowledged. We acknowledge financial support from the European Community in the framework of the network of excellence NANOQUANTA (Contract No. NMP4-CT-2004-500198) and the Deutsche Forschungsgemeinschaft (Project No. Be1346/18-2). Furthermore, we thank the Höchstleistungs Rechenzentrum München for their grant.

[1] Z. M. Jarzebski, Phys. Status Solidi A **71**, 13 (1982).
[2] X. Y. Kong and Z. L. Wang, Solid State Commun. **128**, 1 (2003).
[3] Y. Li, Y. Bando, and D. Goldberg, Adv. Mater. (Weinheim, Ger.) **15**, 581 (2003).
[4] F. Matino, L. Persano, V. Arima, D. Pisignano, R. I. R. Blyth, R. Cingolani, and R. Rinaldi, Phys. Rev. B **72**, 085437 (2005).
[5] S. P. Harvey, T. O. Mason, Y. Gassenbauer, R. Schafranek, and A. Klein, J. Phys. D **39**, 3959 (2006).
[6] Y. Gassenbauer and A. Klein, J. Phys. Chem. B **110**, 4793 (2006).
[7] A. Klein, Appl. Phys. Lett. **77**, 2009 (2000).
[8] Y. Gassenbauer, R. Schafranek, A. Klein, S. Zafeiratos, M. Hävecker, A. Knop-Gericke, and R. Schlögl, Phys. Rev. B **73**, 245312 (2006).
[9] H. Odaka, S. Iwata, N. Taga, S. Ohnishi, Y. Kaneta, and Y. Shigesato, Jpn. J. Appl. Phys., Part 1 **36**, 5551 (1997).
[10] I. Tanaka, M. Mizuno, and H. Adachi, Phys. Rev. B **56**, 3536 (1997).
[11] O. N. Mryasov and A. J. Freeman, Phys. Rev. B **64**, 233111 (2001).
[12] P. Erhart, A. Klein, R. G. Egdell, and K. Albe, Phys. Rev. B **75**, 153205 (2007).
[13] S. Z. Karazhanov, P. Ravindran, P. Vajeeston, A. Ulyashin, T. G. Finstad, and H. Fjellvag, Phys. Rev. B **76**, 075129 (2007).
[14] W. G. Aulbur, L. Jönsson, and J. W. Wilkins, *Solid State Physics: Advances in Research and Applications* (Academic, San Diego, CA, 2000), Vol. 54, p. 1.
[15] S.-H. Wei and A. Zunger, Phys. Rev. B **37**, 8958 (1988).
[16] J. Furthmüller, P. H. Hahn, F. Fuchs, and F. Bechstedt, Phys. Rev. B **72**, 205106 (2005).
[17] Y. Mi, H. Odaka, and S. Iwata, Jpn. J. Appl. Phys., Part 1 **38**, 3453 (1999).
[18] G. Kresse and J. Furthmüller, Phys. Rev. B **54**, 11169 (1996).
[19] G. Kresse and J. Furthmüller, Comput. Mater. Sci. **6**, 15 (1996).
[20] M. Shishkin and G. Kresse, Phys. Rev. B **74**, 035101 (2006).
[21] P. E. Blöchl, Phys. Rev. B **50**, 17953 (1994).
[22] G. Kresse and D. Joubert, Phys. Rev. B **59**, 1758 (1999).
[23] H. J. Monkhorst and J. D. Pack, Phys. Rev. B **13**, 5188 (1976).
[24] P. Hohenberg and W. Kohn, Phys. Rev. **136**, B864 (1964).
[25] W. Kohn and L. J. Sham, Phys. Rev. **140**, A1133 (1965).
[26] J. P. Perdew and A. Zunger, Phys. Rev. B **23**, 5048 (1981).
[27] P. E. Blöchl, O. Jepsen, and O. K. Andersen, Phys. Rev. B **49**, 16223 (1994).
[28] H. Ehrenreich and M. H. Cohen, Phys. Rev. **115**, 786 (1959).
[29] L. Hedin and S. Lundqvist, *Solid State Physics* (Academic, New York, 1969), Vol. 23, p. 1.
[30] F. Fuchs, J. Furthmüller, F. Bechstedt, M. Shishkin, and G. Kresse, Phys. Rev. B **76**, 115109 (2007).
[31] J. Heyd, G. E. Scuseria, and M. Ernzerhof, J. Chem. Phys. **118**, 8207 (2003).
[32] V. I. Anisimov, J. Zaanen, and O. K. Andersen, Phys. Rev. B **44**, 943 (1991).
[33] S. L. Dudarev, G. A. Botton, S. Y. Savrasov, C. J. Humphreys, and A. P. Sutton, Phys. Rev. B **57**, 1505 (1998).
[34] *ICSD, Inorganic Crystal Structure Database* (Fachinformationszentrum Karlsruhe, Germany, 2002).
[35] I. Tanaka, K. Tatsumi, M. Nakano, H. Adachi, and F. Oba, J. Am. Ceram. Soc. **85**, 68 (2002).
[36] F. D. Murnaghan, Proc. Natl. Acad. Sci. U.S.A. **30**, 244 (1944).
[37] P. Vinet, J. Ferrante, J. Rose, and J. Smith, J. Geophys. Res. **92**, 9319 (1987).
[38] M. Sorescu, L. Diamandescu, D. Tarabasanu-Mihaila, and V. S. Teodurescu, J. Mater. Sci. **39**, 675 (2004).
[39] C. Y. Wang, V. Cimalla, H. Romanus, T. Kups, G. Ecke, T. Stauden, M. Ali, V. Lebedev, J. Petzoldt, and O. Ambacher, Appl. Phys. Lett. **89**, 011904 (2006).
[40] A. Schleife, F. Fuchs, J. Furthmüller, and F. Bechstedt, Phys. Rev. B **73**, 245212 (2006).
[41] I. Hamberg, C. G. Granqvist, K. F. Berggren, B. E. Sernelius, and L. Engström, Phys. Rev. B **30**, 3240 (1984).
[42] B. Adolph, V. I. Gavrilenko, K. Tenelsen, F. Bechstedt, and R. Del Sole, Phys. Rev. B **53**, 9797 (1996).